Journal of Quantitative Spectroscopy & Radiative Transfer 167 (2015) 126–134

Contents lists available at ScienceDirect

Journal of Quantitative Spectroscopy & Radiative Transfer

journal homepage: www.elsevier.com/locate/jqsrt

High-resolution absorption measurements of NH_3 at high temperatures: 500–2100 cm^{-1}

Emma J. Barton [a], Sergei N. Yurchenko [a], Jonathan Tennyson [a,*], Sønnik Clausen [b], Alexander Fateev [b]

[a] Department of Physics and Astronomy, University College London, London WC1E 6BT, UK
[b] Technical University of Denmark, Department of Chemical and Biochemical Engineering, Frederiksborgvej 399, 4000 Roskilde, Denmark

ARTICLE INFO

Article history:
Received 20 June 2015
Accepted 28 July 2015
Available online 7 August 2015

Keywords:
High temperature
Ammonia
Absorption
FTIR spectroscopy
High-temperature flow gas cell
Line assignments

ABSTRACT

High-resolution absorption spectra of NH_3 in the region 500–2100 cm^{-1} at temperatures up to 1027 °C and approximately atmospheric pressure (1013 ± 20 mbar) are measured. NH_3 concentrations of 1000 ppm, 0.5% and 1% in volume fraction were used in the measurements. Spectra are recorded in high temperature gas flow cells using a Fourier Transform Infrared (FTIR) spectrometer at a nominal resolution of 0.09 cm^{-1}. Measurements at 22.7 °C are compared to high-resolution cross sections available from the Pacific Northwest National Laboratory (PNNL). The higher temperature spectra are analysed by comparison to a variational line list, BYTe, and experimental energy levels determined using the MARVEL procedure. Approximately 2000 lines have been assigned, of which 851 are newly assigned to mainly hot bands involving vibrational states as high as $v_2=5$.

1. Introduction

Hot planets, cool stars and high temperature industrial processes have molecules (and temperatures) of interest in common. NH_3 is one such molecule.

In smoke stacks NH_3 is used post-combustion to convert highly reactive nitrogen oxides (NOx) into free nitrogen and water vapour through selective catalytic and non-catalytic reduction (SCR and SNCR) [1]. This process must be monitored closely as any un-reacted NH_3, referred to as 'ammonia slip' [2], can cause fouling and corrosion of downstream components and contamination of fly ash [3]. NH_3 is also used throughout the chemical industry, its most important use being for the production of nitric acid [4].

From an astronomical perspective NH_3 has been detected in multiple environments. Cool environments include nearby molecular cloud MBM 12 [5], the comae of comet 10P/Tempel 2 [6], and solar system planets [7]. The presence of NH_3 in the atmospheres of Neptune and Jupiter suggests that it is also likely to be present in the atmospheres of extrasolar giant planets [8]. Hot environments include brown dwarfs (see for example [9]). NH_3 is a significant source of opacity in the infrared spectra of late type T dwarfs, see for example [10], and is expected to be even more important in recently discovered Y dwarfs [11,12]. In fact NH_3 features identified in the near-infrared spectrum of a T dwarf played a significant role in the justification of the Y spectral class [10,11].

The conditions, chemical reactions and gas mixing in industrial processes involving combustion can be monitored by in situ measurements of gas temperature and composition. This can be done spectroscopically, though the result is highly dependent on the quality of reference data [13]. Analysis of brown dwarfs and other such objects using model atmospheres also requires reliable line lists [10].

A hot variational line list for NH_3 called BYTe is available [14] and has been proven to be an effective tool

* Corresponding author.
E-mail address: j.tennyson@ucl.ac.uk (J. Tennyson).

http://dx.doi.org/10.1016/j.jqsrt.2015.07.020
0022-4073/

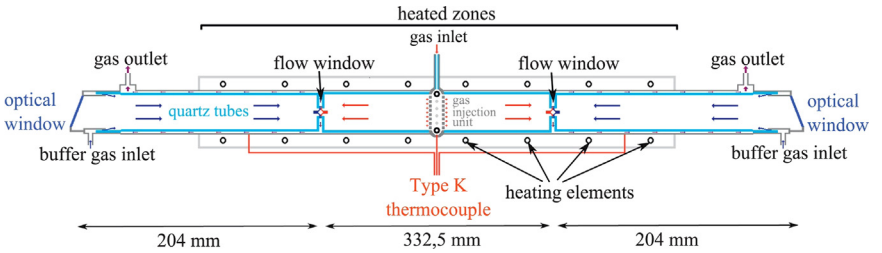

Fig. 1. High temperature quartz gas flow cell (q-HGC) used in the experiments. The red arrows indicate the hot reactive gases, while the blue arrows show the colder buffer gas. Reproduced from [35]. (For interpretation of the references to colour in this figure caption, the reader is referred to the web version of this paper.)

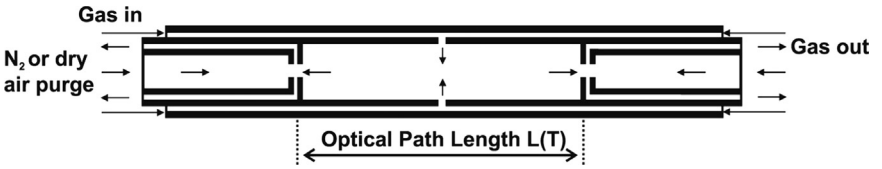

Fig. 2. High temperature ceramic gas flow cell (c-HGC) used in the experiments. Black arrows indicate flow direction. Reproduced from [38].

for the analysis of the tetraatomic molecules' spectrum [15]. BYTe is a variationally computed line list for hot NH_3 that covers the range 0–12,000 cm^{-1} and is expected to be fairly accurate for all temperatures up to 1500 K (1226 °C). It comprises 1,138,323,251 transitions constructed from 1,373,897 energy levels lying below 18,000 cm^{-1}. It was computed using the NH3-2010 potential energy surface [16], the TROVE ro-vibrational computer program [17] and an *ab initio* dipole moment surface [18].

However there is motivation to improve the present line list, which in particular is known to be less accurate for higher frequency transitions [19–21]. During the data analysis presented below we note some frequency shifts and some systematic underestimation of intensities for strong lines in the BYTe lines in comparison to experiment (see Section 4.2). Assigned high resolution laboratory spectra are needed to refine and validate theoretical line positions and intensities.

Numerous studies have endeavoured to assign cold (for example [22–24]) and hot (for example [25,26,15]) NH_3 spectra, many of which are collected in the HITRAN database [27,28]. This has proven to be a challenge due to the congested and complicated nature of the spectrum. A comprehensive compilation of all measured NH_3 rotational and ro-vibrational spectra can be found in a recent MARVEL study [29]. The MARVEL (measured active rotation–vibration energy levels) algorithm [30,31] simultaneously analyses all available assigned and labelled experimental lines, thus yielding the associated energy levels. The recent study for NH_3 analysed 29,450 measured transitions and yielded 4961 accurately-determined energy levels which mostly lie below 7000 cm^{-1} [29].

High resolution emission spectra of NH_3 up to 1300 °C in the regions 740–2100 cm^{-1} and 1650–4000 cm^{-1} were recorded by Hargreaves et al. [32,33]. Zobov et al. [15] analysed the first region and presented assignments for strong lines whose upper levels belong to vibrational states with band origins up to 2100 cm^{-1}. The present work is complementary to these previous works, providing high resolution absorption spectra of NH_3 up to 1027 °C in the region 500–2100 cm^{-1} including assignments. A proportion of these line assignments are new, of which some lines are also present but unassigned in the emission spectra. The notable advantage of our measurements is the absolute intensity scale, as emission intensities are notoriously difficult to calibrate [32–34].

This paper has the following structure. Section 2 describes the experimental setup used for the measurements. Section 3 gives an overview of the method used to calculate experimental and theoretical absorbance spectra and the assignment procedure. Section 4 comes in three parts. The experimental spectrum at 22.7 °C is compared to high resolution PNNL spectra to verify the performance of the whole experimental setup in Section 4.1. The accuracy of BYTe is assessed in Section 4.2 by a direct comparison with the experimental spectra. A summary of all assignments is presented in Section 4.3. Finally Section 5 gives our conclusions and discusses avenues for further work.

2. Experimental details

Measurements up to 500 °C were performed using a quartz high-temperature gas-flow cell (q-HGC) (see Fig. 1) validated for high resolution measurements at temperatures up to 500 °C in the ultra-violet (UV) and infrared (IR) regions [35]. This q-HGC has previously been used to measure absorption cross-sections of various gases (e.g. SO_2) up to 773 K (500 °C) [35]. Measurements above 500 °C were performed using a ceramic high-temperature gas-flow cell (c-HGC) (see Fig. 2) that has also been used by the DTU group [36–38] to study e.g. hot CO and to validate HITEMP2010 [39] for CO_2 and H_2O respectively. This cell operates at temperatures up to 1873 K (1600 °C) [40].

Both cells have the same basic design, three sections separated by flow windows, a fully heated central part and two partially heated buffer parts with interchangeable optical windows at the ends. The buffer parts compensate for heat losses at the ends of the sample cell so as to obtain

a uniform temperature along the length of the central part where absorption measurements are performed. Temperature stability along the axis of the hot part of the cell has been verified using thermocouple measurements and determined to be better than $\pm 1.84\,^{\circ}C$ [35] or $\pm\ 1\,^{\circ}C$ [38] for the q-HGC and c-HGC respectively.

The sample gas (e.g. $N_2+\ NH_3$) is preheated and fed into the middle part of the cell while the buffer parts are purged with carrier gas (e.g. N_2) or dry air taken from a purge generator. The two gas flows meet and form flow windows between the central and outer parts. Here a laminar flow sheet is established meaning the sample gas cannot reach, or react with or form deposits on, the optical windows [41]. The sample gas may still react with the internal surface of the gas cell. To minimise this the inner walls of the q-HGC are made from quartz and those of the c-HGC from high quality pure ceramic (Al_2O_3 (99.5%)). Bottles of premixed gas mixtures, N_2+NH_3 (1000 ppm) and N_2+NH_3 (1%), were obtained from AirLiquid. The purity of the N_2 and NH_3 in the gas bottles was 99.1% with H_2O being the main impurity. High purity N_2 (99.998%) has been used in reference measurements.

Further details on the q-HGC and its performance can be found in [35]. Further details on the c-HGC, its performance and a comparison with the other HGCs in the laboratory will be presented in [40]. For now the reader is referred to [38].

Fig. 3 shows a principle scheme of the optical setup for the absorption measurements. An Aligent 660 FTIR spectrometer, linearised Mercury-Cadmium Telluride (MCT) detector and an external IR light source, which is Blackbody-like (BB) at 1500 K, was used in the measurements on the q-HGC. The optical absorption path length, as confirmed by previous measurements [35], is defined by the flow windows and has a value of 33.25 cm. In the measurements using the c-HGC an external IR light source at 1800 K was used. The absorption path length, again defined by the flow windows, has a value of 53.3 cm. In all experiments KBr windows have been used. These allow spectral measurements in the range 450–40,000 cm^{-1}.

Aligents ResolutionsPRO software (Aligent) calculates the single beam (SB) spectra from the measured interferograms at a nominal resolution of 0.09 cm^{-1} using Fast Fourier Transformation (FFT) and certain apodization functions. Mertz phase correction is applied. Triangular and boxcar apodization functions were used. Boxcar apodization gives narrower peaks but results in more noise in the final spectra. Both sets of calculated SB spectra were used in the final analysis to ensure consistent results.

In accordance with the discussion in [38], measured wavenumbers were multiplied by a factor of 1.000059 to account for the linear wavenumber shift caused by beam divergence. The experimental uncertainties on absorbance measurements are estimated to be within 0.5% [38].

3. Data analysis

This study used the BYTe [14] variational line list and experimental energies determined using the MARVEL procedure [29].

3.1. Calculating experimental absorption spectra

The strategy for calculating experimental transmission spectra $\tau_{exp}(\nu,T)$ at a temperature T [K] and a frequency ν [cm^{-1}] follows [36]

$$\tau_{exp}(\nu,T)=\frac{\mathbf{I}_{gas+BB}-\mathbf{I}_{gas}}{\mathbf{I}_{ref+BB}-\mathbf{I}_{ref}} \quad (1)$$

where $\mathbf{I}_{gas+BB}$ and $\mathbf{I}_{gas}$ are SB sample spectra (N_2+NH_3 mixture) with and without signal from the BB (1500 K or 1800 K), respectively and $\mathbf{I}_{ref+BB}$ and $\mathbf{I}_{ref}$ are SB reference spectra (pure N_2) with and without signal from the BB, respectively. In the case of q-HGC the $\mathbf{I}_{gas}$ and $\mathbf{I}_{ref}$ have been measured by the blocking of the light by a beam-stopper at 23 °C, whereas in the case of c-HGC the moveable mirror in the BB adapter is used to redirect the light to the cold BB source. The absorption spectra are then calculated as

$$A_{exp}(\nu,T)=\log_{10}\left[\frac{a_0}{a_1}\right] \quad (2)$$

where a_0 ($=\mathbf{I}_{ref+BB}-\mathbf{I}_{ref}$) are the reference measurements and a_1 ($=\mathbf{I}_{gas+BB}-\mathbf{I}_{gas}$) are the sample measurements.

Three different absorbance spectra were calculated:

$$A^{a_0}_{exp}(\nu,T)=\log_{10}\left[\frac{a_0}{a_1}\right] \quad (3)$$

$$A^{a^t_0}_{exp}(\nu,T)=\log_{10}\left[\frac{a^t_0}{a_1}\right] \quad (4)$$

$$A_{base}(\nu,T)=\log_{10}\left[\frac{a^t_0}{a_0}\right] \quad (5)$$

where a_0 are reference measurements taken before the sample gas measurements, a_1 are the sample gas measurements and a^t_0 are reference measurements taken after the sample gas measurements. A_{base} was computed to check the baseline. Fig. 4 shows the stability of the baseline before and

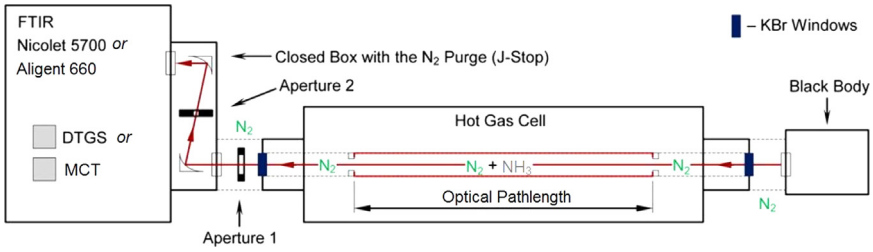

Fig. 3. Experimental setup for the high-resolution measurements of NH_3 at high temperatures. Adapted from [38].

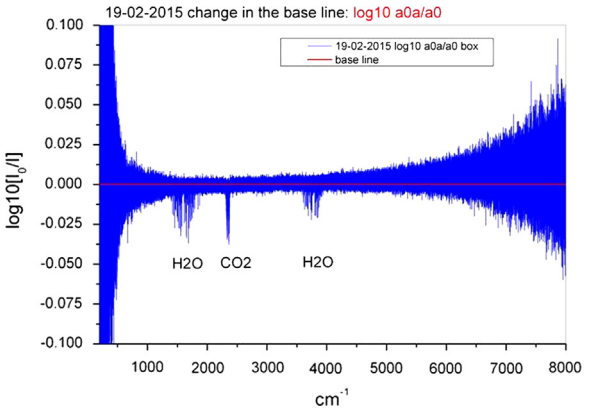

Fig. 4. Stability of the base line before (a_0) and after (a_0^t) measurements with NH_3. The base line (blue) is the same as a theoretical one (red i.e. "0"), except for the H_2O/CO_2 bands. The blue line with negative H_2O/CO_2 trace absorption shows that during the measurements some traces of H_2O/CO_2 have been removed from the gas cell/lines. Noisy parts ($<900\,cm^{-1}$ and $>6000\,cm^{-1}$) are due to low signal level on the detector. Spectral resolution $>0.09\,cm^{-1}$. (For interpretation of the references to colour in this figure caption, the reader is referred to the web version of this paper.)

after the sample gas measurements. The difference between NH_3 absorption spectra $A_{exp}^{a_0}$ and $A_{exp}^{a_0^t}$ is demonstrated in Fig. 5. If the reference a_0 spectrum is used to calculate NH_3 absorption spectrum, then some negative absorption is observed because of H_2O/CO_2 lines. Whereas if the reference a_0^t spectrum is used to calculate NH_3 absorption spectrum, no negative signal is observed. The absence of negative features is preferable, as they can obscure the wings of positive features, however it is possible to use the negative H_2O lines to fine-tune the positions of the positive NH_3 lines, if one believes that the position accuracy for the H_2O lines is high.

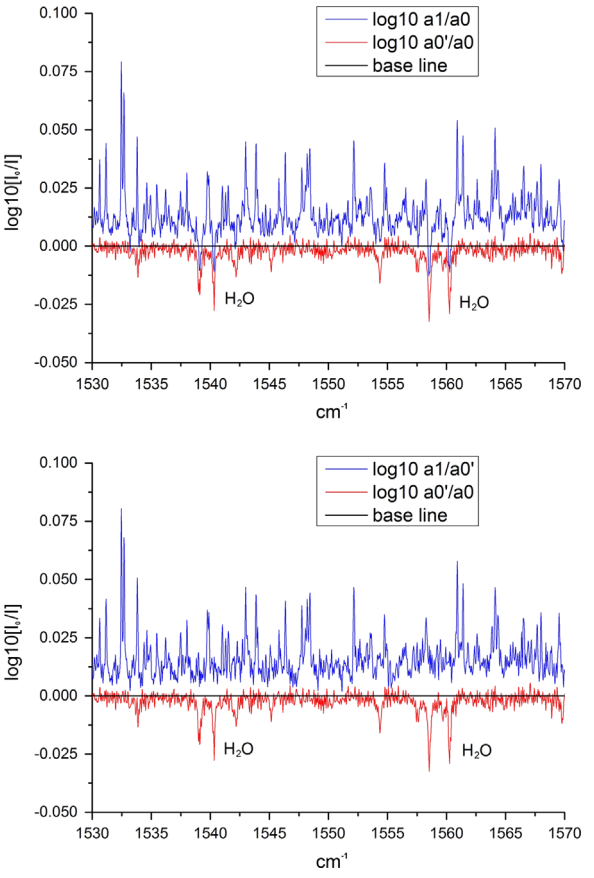

Fig. 5. Absorption spectra (blue, higher spectra) $A_{exp}^{a_0}$ (upper plot) and $A_{exp}^{a_0^t}$ (lower plot) compared to A_{base} (red, lower spectra). Negative features due to H_2O are indicated. (For interpretation of the references to colour in this figure caption, the reader is referred to the web version of this paper.)

3.2. Calculating theoretical absorption spectra

Pressure-broadened NH_3 absorption cross-sections $\sigma(\nu,T)$ were calculated using BYTe and the procedure laid out in [42] but replacing the Gaussian line shape with a Voigt line shape. Lorentz half-widths were estimated from the experimental spectra and with reference to measured widths compiled in the HITRAN database. A transmittance spectrum was calculated from the cross-sections, taking into account absorption path length l [cm] and NH_3 concentration c [cm^{-3}]:

$$\tau_{calc}^{true}(\nu,T)=\exp(-\sigma(\nu,T)lc) \tag{6}$$

The transmittance spectrum was then convolved with the instrument line shape (ILS) function $\Gamma(\nu-\nu_0)$:

$$\tau_{calc}^{eff}(\nu,T)=\int_0^{\infty}\tau_{calc}^{true}(\nu_0,T)\Gamma(\nu-\nu_0)\,d\nu_0 \tag{7}$$

For boxcar apodization, the ILS is a sinc function:

$$\Gamma(\nu)=\Lambda\,\mathrm{sinc}(\Lambda\pi\nu)=\Lambda\frac{\sin(\Lambda\pi\nu)}{(\Lambda\pi\nu)} \tag{8}$$

For triangular apodization, the ILS is a sinc^2 function:

$$\Gamma(\nu)=\Lambda\,\mathrm{sinc}^2(\Lambda\pi\nu)=\Lambda\frac{\sin^2(\Lambda\pi\nu)}{(\Lambda\pi\nu)^2} \tag{9}$$

where Λ is commonly termed the FTIR retardation and is generally defined as the inverse of the nominal resolution of the spectrometer [43]. Finally the theoretical absorption spectrum was computed as

$$A_{calc}(\nu,T)=\log_{10}\left[\frac{1}{\tau_{calc}^{eff}(\nu,T)}\right] \tag{10}$$

3.3. The assignment procedure

Taking the interpreted accuracies of the measurements and BYTe into account (see Section 5), experimental and theoretical peaks were measured and coupled using python scripts to produce an initial assignment list. In cases where multiple BYTe lines corresponded to a single peak, the peak was assigned to the strongest line.

At this point in the analysis MARVEL energy levels [29] became available and were subsequently used to test the

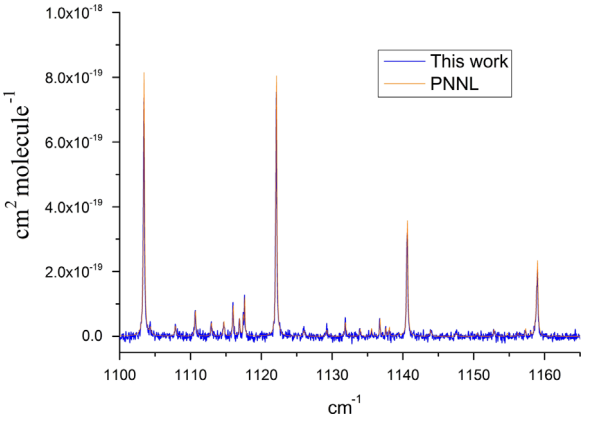

Fig. 6. Comparison between absorption cross-sections at 22.7 °C (this work, blue) and reference absorption spectrum at 25 °C (PNNL, orange). (For interpretation of the references to colour in this figure caption, the reader is referred to the web version of this paper.)

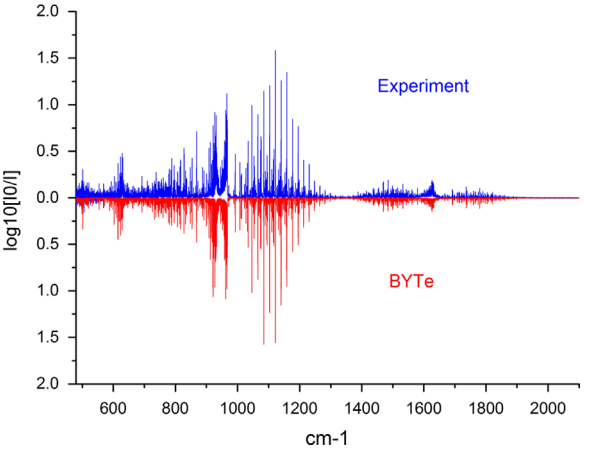

Fig. 7. Comparison between experimental (blue) and calculated (BYTe, red) absorption spectra at 500 °C for the range 500–2100 cm^{-1}. (For interpretation of the references to colour in this figure caption, the reader is referred to the web version of this paper.)

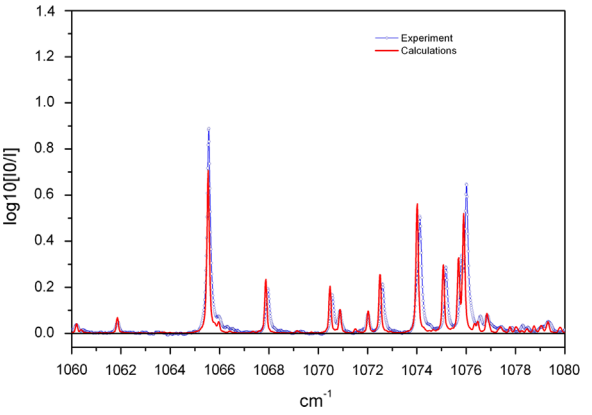

Fig. 8. Comparison between experimental (blue) and calculated (BYTe, red) absorption spectra at 500 °C for the range 1083–1106 cm^{-1}. (For interpretation of the references to colour in this figure caption, the reader is referred to the web version of this paper.)

initial assignment list. Assignments associated with energy levels already determined by experiment may be verified by comparing the line position generated by subtracting upper and lower state energies.

Comparison with MARVEL frequencies led to the identification of several 'problem' BYTe state energies. These energies disagreed with the experimentally derived energies to the extent that their use generated false assignments. In these cases the first step of the assignment procedure was repeated with MARVEL line positions and BYTe intensities to generate intrinsically verified assignments. This is known as trivial assignment.

Any assignments that could not be verified but were not disproved by the comparison to MARVEL line positions were kept as proposed assignments. The reliability of these assignments is discussed in Section 4.3.

A list of all verified and proposed assignments, the final assignment list, was then compared to previous studies, namely those catalogued in the HITRAN database [28] and Zobov et al.'s high-temperature study [15].

4. Results and discussion

The absorption measurements were performed at temperatures of 22.7, 300, 400, 500 and 1027 °C for the NH_3 volume concentrations of 1000 ppm (22.7), 0.5% (300, 400) and 1% (300, 500, 1027). The measurement at 22.7 °C was compared to a high resolution PNNL spectrum while the measurements at 300, 400, 500 and 1027 °C were used to test the accuracy of BYTe then analysed using BYTe to generate an assignment list for the data. The absorption spectra, a composite peak list (partially assigned) for the spectra measured at 1027 °C and new energy level information derived from the assignments are presented in Supplementary Data.

4.1. High-resolution measurements at 22.7 °C

The PNNL database [44] provides high quality reference cross sections for vapour phase infrared spectra obtained using FTIR spectroscopy and pure chemicals. For the data, calculated positional (wavenumber, cm^{-1}) uncertainty is < 0.005 cm^{-1} while the 1σ statistical uncertainty in absorbance values in $< 2\%$. The PNNL NH_3 spectrum at 25 °C is a composite of 12 measurements made at different NH_3 concentrations and a path length of 19.96 cm. Full details on sample conditions, instrument parameters and post-processing parameters are available from PNNL.

The experimental spectrum at 22.7 °C (only one NH_3 concentration) was scaled to the path length of the PNNL spectrum before comparison.

As is illustrated in Fig. 6 there is an excellent agreement between our measurements and the PNNL data, although our data are a little noisy because of the low signal level on the detector and the low NH_3 concentration. The measurements at 22.7 °C have been done in order to compare the current results with available data obtained with about the same class FTIR and (indirectly) check the performance of the whole system (i.e. gas mixing system, gas cell and optical setup).

Table 1
Summary of NH_3 lines assigned in the region 500–2100 cm^{-1}.

Sources	Lines
Experimental	4309
HITRAN	1073
Zobov et al. [15]	43
New trivial	326
New line list	525
Total assigned	1967

4.2. Direct comparison with BYTe

Since BYTe is designed to be used for all temperatures up to 1500 K (1773 °C) [14], it should be ideal for modelling FTIR spectra measured at temperatures of 1027 °C and below. However before proceeding with the analysis it is pertinent to assess the accuracy of the line list. Experimental vs theoretical absorption spectrum at 500 °C for the whole region (500–2100 cm^{-1}) is shown in Fig. 7. In general, taking into account experimental noise, there is good agreement. However taking a closer look at the region 1083–1106 cm^{-1} where the experimental noise is relatively low (<0.01 absorbance) suggests that BYTe is underestimating strong line intensities (by up to 30 %) (Fig. 8). Medium and weak line intensities are reproduced within 20% and 40% respectively. There are also some line position shifts in line positions that are of the order 0.1 cm^{-1} but reach up to 0.5 cm^{-1} in other regions. The comparison suggests that the BYTe line list is accurate to within 0.5 cm^{-1} in line position, at least in the region 500–2100 cm^{-1}. This is consistent with the expected accuracy of the line list [14]. Although it is possible to work with this accuracy it did lead to some false assignments in dense regions, which were identified and corrected partway through the study when the MARVEL results became available. The accuracy of BYTe intensities appears to vary with the strength of individual lines. As such experimental lines were coupled to BYTe lines within 0.5 cm^{-1} using intensity thresholds 30%, 20% and 40% for strong (>0.4 absorbance), medium (>0.1 absorbance) and weak (<0.1 absorbance) lines respectively.

4.3. Assignments

Out of 4309 measured experimental peaks 1967 lines have been assigned: about half of these lines are present in HITRAN. The remaining peaks either did not correspond to a BYTe line within the set wavenumber and intensity thresholds or corresponded to multiple BYTe lines with roughly equal contribution to the total intensity such that it could not be confidently assigned. The partially assigned 1027 °C peak list is presented as Supplementary Data to this paper.

The comparison with previous studies, namely high temperature study [15] and studies compiled in the HITRAN database [28], is shown in Table 1. Of the 851 newly assignment lines, 482 were also present, but unassigned, in [15].

Only 525 of the proposed assignments have the potential to provide new energy level information as, by definition, the upper and lower states of the MARVEL verified assignments are known experimentally. Hence this makes these proposed assignments the most interesting. For proposed assignments with an experimentally known lower energy state, energies for the upper state were computed using MARVEL energies and the frequency of the strongest assigned transition to that state. These are presented as Supplementary Data to this paper.

Lines were assigned to a large number of different bands including bending hot bands up to $5\nu_2$. While being unexpected this is not entirely surprising, as a detailed analysis of hot (1000–1500 °C) H_2O spectra [45–47] produced similar results. Table 2 gives a summary of the observed bands including the number of lines assigned to each and, if the band was observed for the first time in this work, whether this number includes trivial assignments. For simplicity abbreviated vibrational labels ($\nu_1\nu_2\nu_3^{L_3}\nu_4^{L_4}i$) are used to identify bands in this table and only the highest value of the rotational quantum number J assigned in this work for each band is indicated. The full 26 quantum labels for each transition, 13 per vibration-rotation state as recommended by Down et al. [27], are given in the Supplementary Data.

Our 1027 °C spectrum of certain previously observed bands, such as $2\nu_2$ and ν_4^1, has some higher J transitions than previously reported. For these MARVEL energies were used to provide a guideline observed-calculated difference to facilitate reliable line list (proposed) assignments beyond the known J values using the method of branches [48].

17 bands have been observed for the first time in this work, although some of the energy levels involved are experimentally known from measurements of other bands.

If many lines (>10) were assigned to a new band, we were able to track observed-calculated differences through the band. As these remained relatively stable we have confidence in our assignments. Furthermore if a subset of the assignments were trivial we were able to use the same technique as for previously observed bands to ensure our proposed assignments were sensible.

New bands to which only a few assignments could be made are more tentative.

5. Summary

High-resolution absorption measurements of NH_3 in the region 500–2100 cm^{-1} at atmospheric pressure and temperature of 300, 400, 500 and 1027 °C have been reported and analysed. A comparison of the measurements at 22.7 °C with the composite NH_3 spectrum from the PNNL database shows excellent agreement.

A comparison between the measurements and BYTe shows in general good agreement though there are some shifts in line position (up to 0.5 cm^{-1}) and BYTe has some difficulty reproducing strong line intensities. Work towards a new NH_3 line list is currently being carried out as part of the ExoMol project [49].

The use of BYTe and MARVEL has allowed the assignment of 1967 lines. 1116 lines were previously assigned, 1073 by studies included in the HITRAN database and an additional 43 by high temperature study [15]. 851 lines

Table 2
Summary of observed bands in order of theoretical (BYTe) vibrational band centre (VBC = VBO′ − VBO″ where VBO = vibrational band origin) with abbreviated ($v_1v_2v_3^{L_3}v_4^{L_4}i$), vibrational labels and maximum upper and lower J rotational (J'_{max} and J''_{max} respectively) quantum number. N is the number of lines assigned to the band. If J_{max} in this work is higher than that given in the literature, the previously known J_{max} is given in parentheses. iMV indicates a new band with trivial assignments.

Band	VBC	N	J'_{max}	J''_{max}	Note
0^+-0^-	−0.793016[a]	1	28	27	
0^--0^+	0.793016	2	27	26	
$2v_2^+-v_4^{1,-}$	254.80606	5	16	15	
$2v_2^--2v_2^+$	284.696502	14	19	18	
$(2v_2+v_4^1)^--(2v_2+v_4^1)^+$	313.043262	1	10	9	New Band
$(3v_2+v_4^1)^--4v_2^-$	466.768801	1	9 (None)	8	New Band
$3v_2^+-2v_2^-$	501.978729	58	23 (14)	23 (22)	
$(3v_2+v_4^1)^+-(2v_2+v_4^1)^-$	504.649129	11	17 (None)	17	New Band
$3v_2^+-3v_2^-$	511.366446	89	22 (13)	22 (14)	New Band iMV
$(3v_2+v_4^1)^--(3v_2+v_4^1)^+$	522.929054	13	16 (None)	16 (None)	New Band
$(3v_2+v_4^1)^+-4v_2^-$	544.263409	2	12 (None)	12 (7)	New Band
$4v_2^--(2v_2+v_4^1)^-$	560.066366	4	10 (None)	10	New Band
$4v_2^+-3v_2^-$	566.943220	72	21 (7)	21 (13)	New Band iMV
$4v_2^--4v_2^+$	599.680646	14	16 (None)	16 (7)	New Band
$(2v_2+v_4^1)^+-(v_2+v_4^1)^-$	602.916749	34	17 (11)	17 (13)	
$(2v_2+v_4^1)^--3v_2^-$	606.552500	1	13	13	New Band
$2v_2^+-v_2^-$	629.360589	120	24 (20)	24	
$5v_2^+-4v_2^-$	633.065737	4	10 (None)	9 (7)	New Band
$v_4^{1,+}-v_2^-$	658.157170	1	17	16	
$v_4^{1,-}-v_2^-$	659.253867	50	21 (18)	20	
$5v_2^+-(3v_2+v_4^1)^-$	688.482974	1	11 (None)	10 (None)	New Band
$2v_2^--v_2^-$	896.853859	2	16	15	
$(v_2+2v_4^0)^+-2v_4^{0,-}$	898.073060	2	7	6	
$(v_2+v_4^1)^+-v_4^{1,-}$	913.167342	68	19 (13)	18	
$(v_2+v_4^1)^+-v_4^{1,+}$	914.264039	2	19 (13)	18	
$(2v_2+v_4^1)^--(v_2+v_4^1)^+$	915.960012	24	16	16 (13)	
$4v_2^+-(v_2+v_4^1)^+$	922.721046	1	13 (7)	13	New Band
$v_2^+-0^-$	932.438362	208	24	23	
$(v_2+v_4^1)^+-2v_2^+$	948.056868	14	18 (13)	18	
$2v_2^--v_2^+$	949.745375	158	23 (22)	23	
$(v_2+2v_4^2)^--2v_4^{2,+}$	952.951385	2	7	6	
$(v_2+v_4^1)^--v_4^{1,-}$	958.749640	2	14 (13)	13	
$(v_2+v_4^1)^--v_4^{1,+}$	959.846337	62	18 (13)	17	
$v_2^--0^-$	967.329878	2	15	14	
$v_2^--0^+$	968.122894	141	23	22	
$(v_2+v_3^1)^--v_3^{1,+}$	972.941917	4	8	8	
$(v_1+v)^--v_1^+$	983.959104	4	10	9	
$(v_2+v_3^1)^+-v_3^{1,-}$	991.824695	2	9	8	
$3v_2^--v_4^{1,-}$	1267.97613	4	14	14	New Band iMV
$3v_2^--2v_2^+$	1301.041678	23	15 (13)	15	
$3v_2^+-v_2^-$	1398.03582	32	18 (14)	18	
$(v_2+2v_4^0)^+-(v_2+v_4^1)^+$	1575.075800	2	9 (8)	8	
$4v_2^+-2v_2^-$	1580.288396	2	10 (7)	9	New Band iMV
$(v_2+2v_4^0)^--(v_2+v_4^1)^-$	1587.123794	1	6	6	
$2v_4^{0,+}-v_4^{1,+}$	1589.719282	9	12	13	
$2v_4^{0,-}-v_4^{1,-}$	1590.170082	6	12	13	
$(2v_2+v_4^1)^+-2v_2^+$	1591.555915	7	19	18	New Band
$(v_2+2v_4^2)^+-(v_2+v_4^1)^+$	1595.391899	9	17 (7)	16 (13)	
$2v_2^+-0^-$	1597.487235	23	18	18	
$(v_2+2v_4^2)^--(v_2+v_4^1)^-$	1607.009156	1	11 (8)	10	
$(v_2+v_4^1)^+-v_2^+$	1608.105741	67	18 (13)	19	
$2v_4^{2,+}-v_4^{1,+}$	1613.904108	20	14 (11)	15	
$2v_4^{2,-}-v_4^{1,-}$	1614.198476	28	17 (13)	18	
$(v_2+v_4^1)^--v_2^-$	1617.999755	89	19 (13)	20	
$2v_4^{0,-}-2v_2^+$	1619.266592	1	8	9	
$(2v_2+v_4^1)^--2v_2^-$	1619.902676	5	11	12	New Band

Table 2 (*continued*)

Band	VBC	*N*	J'_{max}	J''_{max}	Note
$v_4^{1,+}-0^-$	1625.485696	2	17	17	
$v_4^{1,+}-0^+$	1626.280064	247	20 (18)	20	
$v_4^{1,-}-0^-$	1626.582393	186	21 (18)	22	
$v_4^{1,-}-0^+$	1627.376761	1	6	7	
$2v_4^{2,-}-2v_2^+$	1643.294986	2	14 (13)	13	
$v_1^- - v_4^{1,-}$	1709.695131	1	9	10	
$v_1^+ - v_4^{1,+}$	1701.788598	2	9	10	
$v_3^{1,+}-v_4^{1,+}$	1817.344229	1	6	5	

[a] VBO of 0^+ is set to 0.000000 cm^{-1} in line with the MARVEL study [29].

have been assigned for the first time in this work, 482 were also present but unassigned in the spectra analysed by [15]. The 326 new assignments verified by comparison with MARVEL energy levels, also known as trivial assignments, are secure as the accuracy of MARVEL energies is at least 10^{-4}. Of the 525 proposed assignments, those associated with bands which have verified assignments in this work or numerous assignments should be reliable because the observed-calculated differences remain relatively stable within a given band. The remaining assignments should also be valid, as the method used in this work has proven to be effective at generating valid assignments and reproducing previous work. However caution is advised on the basis that an accuracy of 0.5 cm^{-1} in line position (the accuracy of BYTe) does not rule out miss-assignments.

The NH_3 spectrum between 500 and 2100 cm^{-1} has now been comprehensively studied using both hot emission [15] and hot absorption (this work) spectra. It is the intention of the authors to perform a similar analysis for high resolution absorption measurements of NH_3 in the region 2100–5500 cm^{-1} and potentially the hot emission spectra in the 1650–4000 cm^{-1} region presented by Hargreaves et al. [33] which, to the best of our knowledge, has yet to be analysed.

Acknowledgements

This work was supported by a grant from Energinet.dk project N. 2013-1-1027, by UCL through the Impact Studentship Program and the European Research Council under Advanced Investigator Project 267219.

Appendix A. Supplementary data

Supplementary data associated with this paper can be found in the online version at http://dx.doi.org/10.1016/j.jqsrt.2015.07.020.

References

[1] Trimble DC. AIR QUALITY: information on tall smokestacks and their contribution to interstate transport of air pollution. Technical report. GAO U.S. Government Accountability Office, published: May 11. Publicly released: June 10; 2011.

[2] Staudt JE. Measuring ammonia slip from post combustion NOx reduction system. Technical report. Andover Technology Partners, 2000.

[3] Knight G. Selective Catalytic Reduction Technology for the Control of Nitrogen Oxide Emissions from Coal-Fired Boilers, DIANE Publishing, 2008.

[4] European Commission. Large volume inorganic chemicals—ammonia, acids and fertilisers industries. Technical report. Joint Research Centre, reference Document, 2007.

[5] Gomez JF, Trapero J, Pascual S, Patel N, Morales C, Torrelles JM. Ammonia observations of the nearby molecular cloud MBM 12. Mon Not R Astron Soc 2000;314:743–6.

[6] Biver N, Crovisier J, Bockele-Morvan D, Szutowicz S, Lis D, Hartogh P, et al. Ammonia and other parent molecules in comet 10P/Tempel 2 from Herschel/HIFI and ground-based radio observations. Astron Astrophys 2012;539:A68.

[7] Woodman JH, Trafton L, Owen T. The abundances of ammonia in the atmospheres of Jupiter, Saturn, and Titan. Icarus 1977;32:314–20.

[8] Sudarsky D, Burrows A, Hubeny I. Theoretical spectra and atmospheres of extrasolar giant planets. Astrophys J 2003;588:1121.

[9] Zahnle KJ, Marley MS. Methane, carbon monoxide, and ammonia in brown dwarfs and self-luminous giant planets. Astrophys J 2015;701:L20.

[10] Canty JI, Lucas PW, Tennyson J, Yurchenko SN, Leggett SK, Tinney CG, et al. Methane and ammonia in the near-infrared spectra of late T dwarfs. Mon Not R Astron Soc 2015;450:454–80. http://dx.doi.org/10.1093/mnras/stv586.

[11] Cushing MC, Kirkpatrick JD, Gelino CR, Griffith RL, Skrutskie MF, Mainzer A, et al. The discovery of Y dwarfs using data from the wide-field infrared survey explorer (WISE). Astrophys J 2011;743:50.

[12] Lucas PW, Tinney CG, Burningham B, Leggett SK, Pinfield DJ, Smart R, et al. The discovery of a very cool, very nearby brown dwarf in the Galactic plane. Mon Not R Astron Soc 2010;408:L56–60.

[13] Fateev A, Clausen S. High-resolution spectroscopy of gases at elevated temperatures for industrial applications. In: 22nd UCL astrophysics colloquium: opacities in cool stars and exoplanets; 2012.

[14] Yurchenko SN, Barber RJ, Tennyson J. A variationally computed hot line list for NH_3. Mon Not R Astron Soc 2011;413:1828–34.

[15] Zobov NF, Shirin SV, Ovsyannikov RI, Polyansky OL, Yurchenko SN, Barber RJ, et al. Analysis of high temperature ammonia spectra from 780 to 2100 cm^{-1}. J Mol Spectrosc 2011;269:104–8.

[16] Yurchenko SN, Barber RJ, Tennyson J, Thiel W, Jensen P. Towards efficient refinement of molecular potential energy surfaces: Ammonia as a case study. J Mol Spectrosc 2011;268:123–9.

[17] Yurchenko SN, Thiel W, Jensen P. Theoretical ROVibrational Energies (TROVE): a robust numerical approach to the calculation of rovibrational energies for polyatomic molecules. J Mol Spectrosc 2007;245:126–40. http://dx.doi.org/10.1016/j.jms.2007.07.009.

[18] Yurchenko SN, Barber RJ, Yachmenev A, Thiel W, Jensen P, Tennyson J. A variationally computed $T=300$ K line list for NH_3. J Phys Chem A 2009;113:11845–55.

[19] Huang X, Schwenke DW, Lee TJ. Rovibrational spectra of ammonia. i. unprecedented accuracy of a potential energy surface used with nonadiabatic corrections. J Chem Phys 2011;134:044320.

[20] Huang X, Schwenke DW, Lee TJ. Rovibrational spectra of ammonia. II. Detailed analysis, comparison, and prediction of spectroscopic assignments for $^{14}NH3$, $^{15}NH_3$, and $^{14}ND3$. J Chem Phys 2011;134:044321.

[21] Sung K, Brown LR, Huang X, Schwenke DW, Lee TJ, Coy SL, et al. Extended line positions, intensities, empirical lower state energies and quantum assignments of NH_3 from 6300 to 7000 cm^{-1}. J Quant Spectrosc Radiat Transf 2012;113:1066–83.
[22] Sasada H, Endo Y, Hirota E, Poynter RL, Margolis JS. Microwave and Fourier-transform infrared spectroscopy of the $v_4=1$ and $v_2=2$ states of NH_3. J Mol Spectrosc 1992;151:33–53.
[23] Kleiner I, Brown LR, Tarrago G, Kou Q-L, Picqué N, Guelachvili G, et al. Positions and intensities in the $2\nu_4/\nu_1/\nu_3$ vibrational system of ^{14}NH3 near 3 μm. J Mol Spectrosc 1999;193:46–71.
[24] Cottaz C, Kleiner I, Tarrago G, Brown LR, Margolis JS, Poynter RL, et al. Line positions and intensities in the $2\nu_2/\nu_4$ vibrational system of ^{14}NH3 near 5–7 μm. J Mol Spectrosc 2000;203:285–309.
[25] Cottaz C, Tarrago G, Kleiner I, Brown LR. Assignments and intensities of ^{14}NH3 hot bands in the 5- to 8- μm ($3\nu_2-\nu_2$, $\nu_2+\nu_4-\nu_2$) and 4μm ($4\nu_2-\nu_2$, $\nu_1-\nu_2$, $\nu_3-\nu_2$ and $2\nu_4-\nu_2$) regions. J Mol Spectrosc 2001;209:30–49.
[26] Yu S, Pearson JC, Drouin BJ, Sung K, Pirali O, Vervloet M, et al. Submillimeter-wave and far-infrared spectroscopy of high-J transitions of the ground and $\nu_2=1$ states of ammonia. J Chem Phys 2010;133:174317.
[27] Down MJ, Hill C, Yurchenko SN, Tennyson J, Brown LR, Kleiner I. Re-analysis of ammonia spectra: updating the HITRAN $^{14}NH_3$ database. J Quant Spectrosc Radiat Transf 2013;130:260–72.
[28] Rothman LS, Gordon IE, Babikov Y, Barbe A, Benner DC, Bernath PF, et al. The HITRAN 2012 molecular spectroscopic database. J Quant Spectrosc Radiat Transf 2013;130:4–50. http://dx.doi.org/10.1016/jqsrt.2013.07.002.
[29] Al Derzi AR, Furtenbacher T, Yurchenko SN, Tennyson J, Császár AG. MARVEL analysis of the measured high-resolution spectra of ^{14}NH3. J Quant Spectrosc Radiat Transf 2015;161:117–30. http://dx.doi.org/10.1016/j.jqsrt.2015.03.034.
[30] Furtenbacher T, Császár AG, Tennyson J. MARVEL: measured active rotational-vibrational energy levels. J Mol Spectrosc 2007;245:115–25.
[31] Furtenbacher T, Császár AG. MARVEL: measured active rotational-vibrational energy levels. II. Algorithmic improvements. J Quant Spectrosc Radiat Transf 2012;113:929–35.
[32] Hargreaves RJ, Li G, Bernath PF. Ammonia line lists from 1650 to 4000 cm^{-1}. J Quant Spectrosc Radiat Transf 2012;113:670–9.
[33] Hargreaves RJ, Li G, Bernath PF. Hot NH_3 spectra for astrophysical applications. Astrophys J 2012;735:111.
[34] Nassar R, Bernath P. Hot methane spectra for astrophysical applications. J Quant Spectrosc Radiat Transf 2003;82:279–92. http://dx.doi.org/10.1016/S0022-4073(03)00158-4.
[35] Grosch H, Fateev A, Nielsen KL, Clausen S. Hot gas flow cell for optical measurements on reactive gases. J Quant Spectrosc Radiat Transf 2013;130:392–9.
[36] Evseev V, Fateev A, Clausen S. High-resolution transmission measurements of CO_2 at high temperatures for industrial applications. J Quant Spectrosc Radiat Transf 2012;113:2222–33.
[37] Bercher V, Clausen S, Fateev A, Spliethoff H. Oxyfuel combustion. Int Greenhouse Gas Control 2011;5:S76–99.
[38] Alberti M, Weber R, Mancini M, Fateev A, Clausen S. Validation of HITEMP-2010 for carbon dioxide and water vapour at high temperatures and atmospheric pressure in 450–7600 cm^{-1} spectral range. J Quant Spectrosc Radiat Transf 2015;157:14–33.
[39] Rothman LS, Gordon IE, Barber RJ, Dothe H, Gamache RR, Goldman A, et al. HITEMP, the high-temperature molecular spectroscopic database. J Quant Spectrosc Radiat Transf 2010;111:2139–50.
[40] Clausen S, Nielsen KA, Fateev A. Ceramic gas cell operating up to 1873 K. Meas Sci Technol 2015, in preparation.
[41] Fateev A, Clausen S. Online non-contact gas analysis. Technical report. Technical University of Denmark, contract no.: Energinet.dk no. 2006 1 6382; 2008.
[42] Hill C, Yurchenko SN, Tennyson J. Temperature-dependent molecular absorption cross sections for exoplanets and other atmospheres. Icarus 2013;226:1673–7.
[43] Griffiths PR, de Haseth JA. Fourier transform infrared spectrometry: chemical analysis. New York: John Wiley and Sons; 1986.
[44] Sharpe SW, Johnson TJ, Sams RL, Chu PM, Rhoderick GC, Johnson PA. Gas-phase databases for quantitative infrared spectroscopy. Appl Spectrosc 2004;58:1452–61. http://dx.doi.org/10.1366/0003702042641281.
[45] Polyansky OL, Zobov NF, Tennyson J, Lotoski JA, Bernath PF. Hot bands of water in the ν_2 manifold up to $5\nu_2-4\nu_2$. J Mol Spectrosc 1997;184:35–50.
[46] Zobov NF, Polyansky OL, Tennyson J, Lotoski JA, Colarusso P, Zhang K-Q, et al. Hot bands of water up to $6\nu_2-5\nu_2$ in the 933 - 2500 cm^{-} region. J Mol Spectrosc 1999;193:118–36.
[47] Zobov NF, Shirin SV, Polyansky OL, Tennyson J, Coheur P-F, Bernath PF, et al. Monodromy in the water molecules. Chem Phys Lett 2005;414:193–7.
[48] Polyansky OL, Zobov NF, Viti S, Tennyson J, Bernath PF, Wallace L. K band spectrum of water in sunspots. Astrophys J 1997;489:L205–8.
[49] Tennyson J, Yurchenko SN. ExoMol: molecular line lists for exoplanet and other atmospheres. Mon Not R Astron Soc 2012;425:21–33.